

# Impurity-induced moment freezing in $\text{NaFe}_x\text{Ru}_{1-x}\text{O}_2$

Alon Hendler Avidor,<sup>1,\*</sup> Brenden R. Ortiz,<sup>1,2</sup> Paul M. Sarte,<sup>1</sup> Qiang Zhang,<sup>3</sup> and Stephen D. Wilson<sup>1,†</sup>

<sup>1</sup>*Materials Department, University of California Santa Barbara, Santa Barbara, CA 93106, USA*

<sup>2</sup>*Materials Science and Technology Division, Oak Ridge National Laboratory, Oak Ridge, 37831, Tennessee, USA*

<sup>3</sup>*Neutron Scattering Division, Oak Ridge National Laboratory, Oak Ridge, Tennessee 37831, USA*

(Dated: February 17, 2025)

We report the impact of magnetic impurity substitution on the quantum disordered magnetic ground state of  $\text{NaRuO}_2$ . Local  $S = 5/2$  moments are introduced into the frustrated triangular lattice of  $J_{eff} = 1/2$  Ru moments via Fe-substitution in  $\text{NaFe}_x\text{Ru}_{1-x}\text{O}_2$ , and the evolution of the magnetic ground state is reported. Local spin freezing associated with conventional spin glass behavior is observed upon Fe substitution, marking an impurity-induced freezing of the primarily dynamic magnetic ground state in  $\text{NaRuO}_2$ . Furthermore, local Fe moments induce a Curie-Weiss magnetic behavior in the uniform magnetic susceptibility, and the local moment magnitude is best described by dynamic Ru moments polarized about impurity sites. Our results establish an impurity-doping phenomenology consistent with inherently dynamic moments in  $\text{NaRuO}_2$  that are pinned by local magnetic impurities, similar to “swiss cheese” models of impurity-substituted copper oxides,

## I. INTRODUCTION

Layered oxides with the structure type  $\alpha\text{-NaMO}_2$  where  $M$  is a transition metal or lanthanide ion often host a frustrated triangular lattice of magnetic moments capable of stabilizing a variety of unconventional phenomena. The magnetic layers are composed of  $\text{MO}_6$  edge-sharing octahedra, which are spaced by alkali metal layers. This results in predominantly quasi-two dimensional interactions, and the local orbital and spin configurations of the  $M$ -site ion can drive a wide variety of collective magnetic behaviors. For instance, in the limit of weak spin-orbit coupling, the relatively isotropic  $S = 1/2$  case of  $M=\text{Ti}$  is proposed to form a nonmagnetic orbital dimer state [1] whereas for  $S = 5/2$  moments and  $M=\text{Fe}$  competing exchange interactions drive a complex thermal evolution of magnetic order and short-range correlations [1]. Orbital effects, such as a strong Jahn-Teller distortion in the  $S = 2$ ,  $M=\text{Mn}$  case, can drive the formation of quasi-one dimensional spin correlations and stabilize single-ion anisotropy-driven magnon bound states [2–4], and orbital order can also intertwine with magnetic ordering in the case of  $S = 1$  and  $M=\text{V}$  [5].

The addition of appreciable spin-orbit coupling can introduce further richness into the phase diagrams of these materials. Intrinsically quantum disordered or quantum spin liquid ground states have been reported in a number of spin-orbit entangled  $M$ =lanthanide compounds with  $S_{eff} = 1/2$  ground state wave functions [6–9]. For instance, a number of intrinsically quantum disordered magnetic ground states form in  $\text{NaYbX}_2$  ( $X=\text{O}, \text{S}, \text{Se}$ ) compounds [8, 10–12] and in  $\text{RbCeO}_2$  [13] with well-isolated Kramers doublet ground state wave functions [14–16]. Moving toward the limit of stronger crystal electric fields, the spin-orbit Mott state in  $\text{NaRuO}_2$

also realizes a spin-orbit entangled  $J_{eff} = 1/2$  ground state wave function built from  $t_{2g}$  orbitals with strong anisotropic exchange interactions [17]. Despite predictions of a ferromagnetic ground state [18, 19], an unusual, quantum disordered magnetic ground state forms in this compound—a state marked by persistent low-frequency dynamics and a field-tunable  $\gamma$ -term in the low temperature specific heat.

While the correct starting Hamiltonian for understanding the formation of quantum disorder in  $\text{NaRuO}_2$  remains a topic of investigation, with candidates ranging from Heisenberg-Kitaev- $\Gamma$  models [20] to charge fluctuations inherent to a weak Mott state [21, 22] to extended/ring-exchange effects across the triangular network [23], the fate of local moments within this compound also remains an open question. High-temperature susceptibility data in  $\text{NaRuO}_2$  is dominated by a weakly temperature-dependent Van Vleck response that does not fit to a Curie-Weiss formalism below 400 K [17]. This is likely due to a combination of single-ion Kotani-type effects combined with a strong mean-field term, an analysis challenge that has only recently been addressed in strongly spin-orbit coupled transition metal halides [24]. Nevertheless, a partial freezing of moments is observed below  $\approx 2$  K in  $\text{NaRuO}_2$ , and the origin of this freezing remains an open question.

In particular, whether the weak freezing is driven by a small fraction of impurities or is an intrinsic property of the bulk system are yet to be determined. Prior muon spin relaxation measurements suggest that the freezing occurs throughout the sample [17]; however nonmagnetic defect substitution in the form of local Na defects within the Ru sublattice of  $\text{Na}_{3+x}\text{Ru}_{3-x}\text{O}_6$  also drive clear spin glass freezing with a clear signature in the irreversibility of the susceptibility [25]. Traversing the solid solution  $\text{Na}_{3+x}\text{Ru}_{3-x}\text{O}_6$ , however, is a strong perturbation to the system, where the oxidation state of Ru is altered in parallel to the introduction of in-plane defects. An alternative approach is to introduce magnetic, in-plane disorder into  $\text{NaRuO}_2$  to test the potential for defect-induced spin

\* [hendleravidor@ucsb.edu](mailto:hendleravidor@ucsb.edu)

† [stephendwilson@ucsb.edu](mailto:stephendwilson@ucsb.edu)

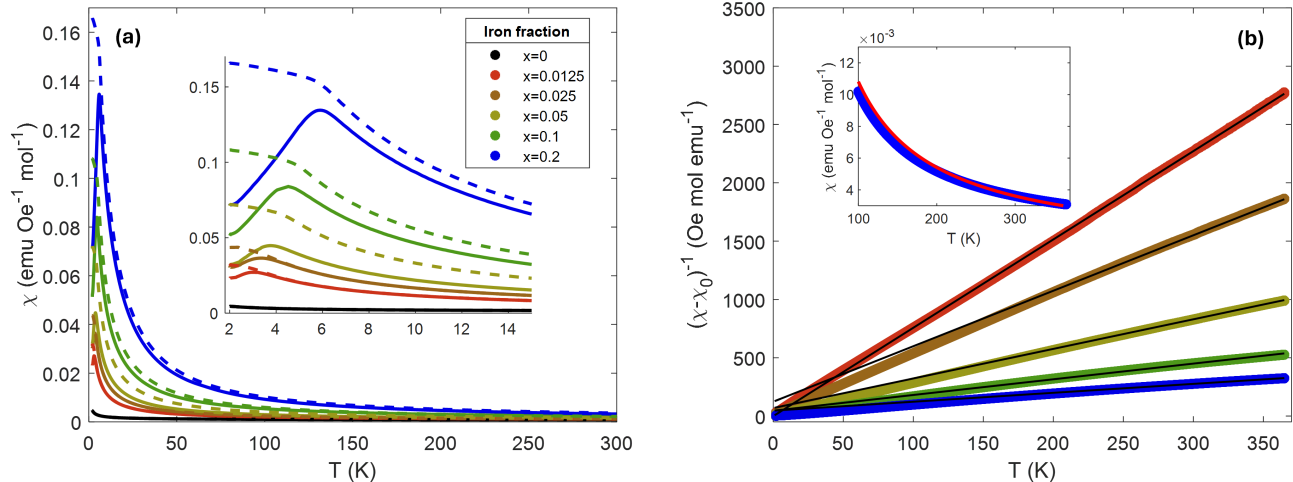


FIG. 1. DC magnetic susceptibility,  $\chi$ , collected under  $H=200$  Oe for the  $\text{NaFe}_x\text{Ru}_{1-x}\text{O}_2$  series. (a)  $\chi$  plotted as a function of temperature showing zero field cooled (ZFC, solid line) and field-cooled (FC, dashed line) data, as well as a peak for the ZFC data in all samples. The inset shows an expanded low temperature region,  $2 < T < 15$  K for greater detail. (b)  $\chi^{-1}$  as a function of temperature collected between 2 K and 365 K. The linear fits are to a Curie-Weiss form of susceptibility as described in the text. The inset shows the fit to the form  $\chi = \chi_0 + C/(T - \Theta_{CW})$   $\chi_0$  is a temperature independent term fit across the entire temperature range.

freezing and also to test the influence of a local moment on the background spin fluctuations.

To address this problem, in this paper we present a study of the magnetic behavior of  $\text{NaRuO}_2$  as isovalent  $\text{Fe}^{3+}$  local moment impurities are introduced into the  $\text{Ru}^{3+}$  triangular lattice network.  $\text{NaRu}_{1-x}\text{Fe}_x\text{O}_2$  samples were created with Fe concentrations ranging between  $0 \leq x \leq 0.2$ , and the evolution of their magnetic properties is explored. Similar to the case of Na-defects introduced into the Ru-planes, Fe-impurities induce a conventional spin freezing at low temperatures, whose onset temperature increases with the degree of disorder. The  $3d^5$   $\text{Fe}^{3+}$   $S = 5/2$  local moment defects further induce a local moment magnetic response at high temperatures that can be modeled within a conventional Curie-Weiss formalism. Surprisingly, the magnitude of the local moment exceeds that of isolated  $\text{Fe}^{3+}$  moments and can instead be modeled assuming polarized neighboring  $\text{Ru}^{3+}$  moments pinned about the impurity sites. Our results suggest that local moments are present in  $\text{NaRuO}_2$  and are bound by either fluctuations or a strong exchange field. Their liberation via in-plane impurities is reminiscent of “swiss cheese” models of impurity-substituted cuprates [26].

## II. EXPERIMENTAL DETAILS

A series of polycrystalline  $\text{NaFe}_x\text{Ru}_{1-x}\text{O}_2$  samples were synthesized using previously reported solid state techniques [25]. Starting mixtures were modified such that  $\text{RuO}_2$  was replaced with  $\text{Fe}_2\text{O}_3$  (Alfa Aesar, 99.99% purity) and the ratio of  $\text{Na}_2\text{O}_2$  and Na was adjusted to

maintain stoichiometry for each target concentration  $x$ . Five samples with  $x = 0.0125, 0.025, 0.05, 0.1$  and  $0.2$  were created, and attempts at larger concentrations of Fe showed signatures of phase separation and a potential miscibility limit of Fe within the matrix. To verify the chemical composition and crystal structure, x-ray fluorescence spectroscopy measurements were performed (Rigaku ZSX Primus IV) and powder x-ray diffraction measurements (Panalytical Empyrean,  $\text{Cu } \lambda = 1.54(\text{\AA})$ ) were performed [27]. These measurements confirmed that the structure maintained a single phase  $R\bar{3}m$  space group as a function of Fe composition and that the target substitution level  $x$  was realized in the final powders. Attempts to prepare the sample series using an alternative method of the reported process for  $\text{NaFeO}_2$  [28] while exchanging a portion of reagent  $\text{Fe}_2\text{O}_3$  with  $\text{RuO}_2$  were unsuccessful. Both DC and AC susceptibility measurements were conducted using a Quantum Design Magnetic Properties Measurement System (MPMS). For AC-susceptibility measurements, all samples were measured with a driving field of 3 Oe at 10, 100, 250, 500 and 700 Hz. Neutron diffraction data were collected using the POWGEN diffractometer at the Spallation Neutron Source at Oak Ridge National lab. Neutron frames 2 and 3 with center wavelengths of 1.5 ( $\text{\AA}$ ) and 2.665 ( $\text{\AA}$ ) were used, respectively, for the data collection. An orange cryostat was adopted as the sample environment to cover the temperature region of 1.6-300 K.

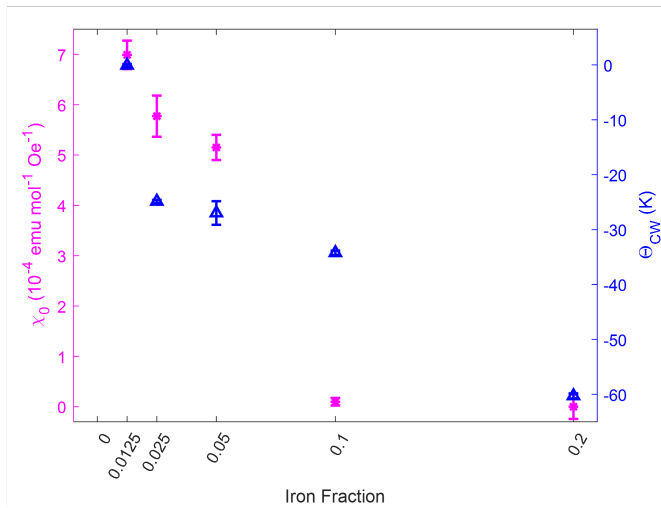


FIG. 2. The Curie-Weiss temperatures  $\Theta_{CW}$  and temperature independent susceptibility  $\chi_0$  extracted from the fits shown in Figure 1 across the entire the  $\text{NaFe}_x\text{Ru}_{1-x}\text{O}_2$  sample series.

$x$	$T_f$ (K)	$\mu_{eff}$ ( $\mu_B$ )	$\mu_{eff}$ ( $\mu_B$ )	$\mu_{eff}$ ( $\mu_B$ )
Fe content		measured	Fe only	Ru and Fe
0.0125	2.93	$1.03 \pm 0.03$	0.66	0.93
0.025	3.32	$1.36 \pm 0.05$	0.93	1.29
0.05	3.80	$1.78 \pm 0.06$	1.32	1.74
0.10	4.52	$2.43 \pm 0.06$	1.87	2.34
0.20	5.93	$3.23 \pm 0.02$	2.64	3.05
1	11	5.80 Ref. [29]	5.91	-

TABLE I. Spin freezing temperatures and effective magnetic moments measured for all  $\text{NaFe}_x\text{Ru}_{1-x}\text{O}_2$  samples. Two models of a paramagnet are added for comparison—the first with only the Fe  $S = 5/2$  spins, and the second with the Fe spins as well as induced Ru  $J_{eff} = 1/2$  moments. The model assumes account the first and second nearest neighbors polarizing, as discussed in the text. For pure  $\text{NaFeO}_2$ , the values are taken from Ichida et al.[29]

### III. EXPERIMENTAL RESULTS

DC magnetization measurements were performed to study the evolution of the magnetic behavior in  $\text{NaFe}_x\text{Ru}_{1-x}\text{O}_2$  with increasing  $x$ . Low-field susceptibility (M/H) data were collected upon warming from 2 K to 300 K at a sweep rate of 2 K/min, using a DC field of 200 Oe after both zero-field cooling (ZFC) and field cooling (FC) conditions. The resulting data are shown in Figure 1 (a). Two qualitative changes are immediately evident in the susceptibility with the introduction of Fe impurities. The first is that magnetic susceptibility is significantly enhanced at all temperatures due to an added Curie-like response, and the second is the appearance of a peak in ZFC conditions which shows irreversibility between FC and ZFC curves. The low temperature behavior is consistent with a disorder-driven spin glass freezing,

which is absent in pure  $\text{NaRuO}_2$  over this temperature regime. For reference,  $\alpha\text{-NaFeO}_2$  orders below  $T_N = 11.1$  K [29], and a subtle irreversibility is also reported at the same temperature, likely due to residual fluctuations into the lower temperature magnetic state [28].

The impurity-induced, high-temperature magnetic susceptibility can be fit via a Curie-Weiss model with a temperature-independent  $\chi_0$  term added. Figure 1 (b) shows the resulting  $(\chi(T) - \chi_0)^{-1}$  data plotted with the fit  $\chi_0$  term removed. A fit range between 200 K and 365 K was used for all samples and linear fits were possible for the entire  $\text{NaFe}_x\text{Ru}_{1-x}\text{O}_2$  series. This reflects the introduction of local moments via the addition of Fe impurities. The effective magnetic moment extracted from the Curie-Weiss fits can then be compared with the expectation of introducing a fraction  $x$  of  $S = 5/2$  moments, while the host material  $\text{NaRuO}_2$  does not show clear Curie-Weiss behavior [17]. Figure 1 (a) also shows the susceptibility for the undoped  $x = 0$  compound for comparison.

As summarized in Table 1, the simplest model of introducing isolated  $S = 5/2$  local moments fails to explain the magnitude of Curie-Weiss moment. The local moment  $\mu_{eff} = g\sqrt{N J(J+1)}$  in units of  $\mu_B$ , where  $N$  is the volume fraction of the  $x$  magnetic moments assuming the previously reported  $g = 2$  [29] and  $J = 5/2$ , is systematically larger throughout the  $\text{NaFe}_x\text{Ru}_{1-x}\text{O}_2$  series. One possible origin of this response is to assume that local moments are present in  $\text{NaRuO}_2$ , yet bound by strong interactions or hidden by strong fluctuations in the measurable temperature regime. The introduction of spin impurities into the Ru triangular lattice can locally freeze and polarize the  $J_{eff} = 1/2$   $\text{Ru}^{3+}$  moments and generate an enhanced  $\mu_{eff}$  per magnetic impurity added.

To test this possibility, a simple Monte Carlo model of  $\text{Fe}^{3+}$  spins spread randomly across the triangular lattice was created, assuming neighboring  $\text{Ru}^{3+}$  moments are polarized out to the nearest neighbor and next-nearest neighbor distances. In this model, assuming each Ru  $J_{eff} = 1/2$  moment contributes  $\mu_{eff} = 1.73 \mu_B$ , the best fit to the total effective moment extracted from Curie-Weiss fits results when Ru moments are polarized up to the next-nearest neighbor about each Fe impurity site. This Monte Carlo approach allows for an approximation of the substitution level at which all Ru moments are polarized at various coordination levels about the Fe-sites and for the determination of the relative fraction of Ru moments polarized at intermediate impurity substitution levels [27].

Figure 2 plots the evolution of the  $\chi_0$  term and  $\Theta_{CW}$  as a function of Fe-content  $x$ .  $\Theta_{CW}$  shows a finite antiferromagnetic value that grows with increasing Fe content up to the  $x = 0.2$  limit. Notably, at this limit,  $\Theta_{CW}$  becomes substantial, reflecting strong interactions between the impurity-induced moment clusters. As this large mean field appears, the  $\chi_0$  term simultaneously vanishes with increasing  $x$ . The large  $\chi_0$  of the parent  $x = 0$  com-

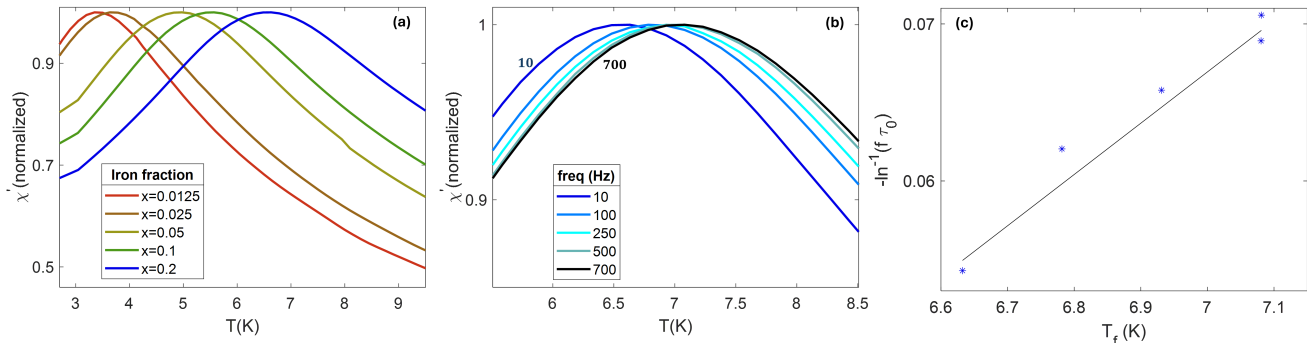


FIG. 3. (a) The AC susceptibility of all samples collected at 10 Hz. The real part of the susceptibility  $\chi'$  is normalized to 1 at its peak and plotted as a function of temperature. (b) The frequency dependence of the peak in  $\chi'$ , labeled as  $T_f$ , is shown for the sample with the largest fraction of iron content,  $\text{NaFe}_{0.2}\text{Ru}_{0.8}\text{O}_2$ .  $T_f$  is shifted upward in temperature upon increasing frequency. (c) The Vogel-Fulcher fit to the frequency dependence of  $T_f$ , shown for the  $\text{NaFe}_{0.2}\text{Ru}_{0.8}\text{O}_2$  sample.

pound [17] is rapidly quenched and vanishes by  $x = 0.1$ , which is a concentration coinciding with nearly all Ru moments being polarized by local Fe impurities in the value for  $\mu_{eff}$ . This is again consistent with a two-phase model of local Fe impurities polarizing an extended halo of Ru moments that rapidly percolates with  $x$ .

Now turning to the lower temperature regime of the measured susceptibility, the freezing behavior shown in the inset of Figure 1 (a) evolves as a function of  $x$ , and the onset of irreversibility  $T_f$  is summarized in Table 1. This transition is better illustrated through AC susceptibility measurements plotted in Figure 3 (a) where the 10 Hz data are normalized to a common peak value and  $T_f$  is seen to reach a maximum of  $\approx 6$  K at  $x = 0.2$ . To illustrate the spin freezing further, the frequency dependence of  $\chi'(T)$  for the  $x = 0.2$  composition is plotted in Figure 3 (b). A clear shift in the cusp is seen upon increasing frequency, which can be parameterized via a standard Vogel-Fulcher analysis [30, 31]. Fits were performed to the form:

$$\tau = \tau_0 e^{(E_a/k_B(T_f - T_0))} \quad (1)$$

Here  $f = \tau^{-1}$  is the frequency,  $T_f$  is the relaxation (freezing) temperature, and there are three phenomenological, system-dependent parameters: characteristic relaxation time  $\tau_0$ , the activation energy  $E_a$ , and the Vogel-Fulcher temperature  $T_0$ , a measure of intercluster interaction strength [32].

Figure 3(c) shows the result of fitting data in panel 3(b) to the Vogel-Fulcher relation. The activation energy can be deduced from the slope in Figure 3 (c):  $E_a/k_B = 30.6$  K which is consistent with reported values for other Fe-based spin glasses [33–35].  $\tau = 10^{-9}$  was obtained, a value more in line with cluster spin glass systems, and larger than atomic spin glass [34–37].

To explore the most heavily doped compound,  $x = 0.2$ , further, neutron powder diffraction measurements were performed. Data were collected across a series of temperatures down to 1.6 K, and no magnetic or crystal-

lographic transitions were observed. The  $E_i = 1.5$  Å measurements for all temperatures are shown in Figure 4. Consistent with a spin glass state below  $T_f$ , no magnetic superlattice reflections were observed or correlated magnetic intensity evident below 6 K. Magnetic diffuse scattering was also not resolved, though the small fraction of  $S = 5/2$  moments would likely preclude its observation. Although no long-range magnetic order was observed, crystallographic information can be determined from the diffraction data, and the lattice and unit cell parameters are summarized in Table II.

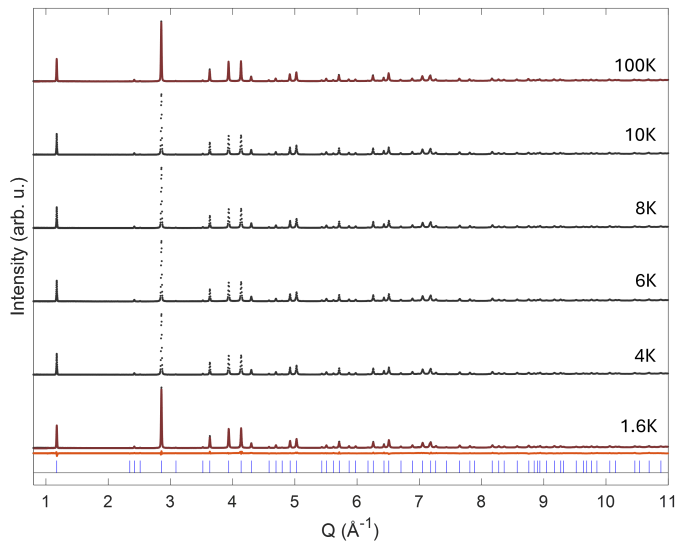


FIG. 4. Neutron diffraction data collected at different temperatures for the iron rich sample  $\text{NaFe}_{0.2}\text{Ru}_{0.8}\text{O}_2$ . Refinement results of the structure are shown for  $T = 1.6$  K and  $T = 100$  K data (red), and the difference between the data and the refined structural model is shown for  $T = 1.6$  K below the data. Tick marks indicate the expected Bragg peak positions for the  $\text{NaRuO}_2$  phase.

	NaRuO <sub>2</sub>	NaFe <sub>0.2</sub> Ru <sub>0.8</sub> O <sub>2</sub>	NaFeO <sub>2</sub>
$T$ (K)	1.5 [17]	1.6	4.2 [38]
$a$ (Å)	3.055	3.036	3.018
$c$ (Å)	16.122	16.052	16.047

Atom	Wyckoff	x	y	z	Occupancy
Fe	3b	0	0	0.5	0.192
Ru	3b	0	0	0.5	0.790
Na	3a	0	0	0	0.925
O	6c	0	0	0.23344(5)	1.0000

TABLE II. The measured lattice parameters of NaFe<sub>0.2</sub>Ru<sub>0.8</sub>O<sub>2</sub>, compared to its two stoichiometric end points: NaRuO<sub>2</sub> taken from Ortiz et al. [17] and NaFeO<sub>2</sub> from Tomkowicz et al. [38]. The temperatures with which the respective measurements were taken are also shown for comparison. Unit cell parameters from Rietveld refinement of NaFe<sub>0.2</sub>Ru<sub>0.8</sub>O<sub>2</sub> with  $R_{exp} = 1.227$  and  $R_{wp} = 8.948$

#### IV. DISCUSSION AND CONCLUSIONS

The structure of NaFe<sub>0.2</sub>Ru<sub>0.8</sub>O<sub>2</sub> remains in the  $R\bar{3}m$  space group, the same as either side of the alloy series NaRuO<sub>2</sub> and NaFeO<sub>2</sub>, both shown in Table II for comparison. The magnetic states at either end of the alloy series are both frustrated by the triangular lattice motif of the transition metal ions; however, the more quantum  $J_{eff} = 1/2$  moments of NaRuO<sub>2</sub> manifest an intrinsically disordered ground state while the more classical moments of NaFeO<sub>2</sub> show a lock-in like transition from incommensurate to commensurate order upon cooling below 8 K [28]. The spin glass freezing of moments in the Fe substituted NaRu<sub>1-x</sub>Fe<sub>x</sub>O<sub>2</sub> is consistent with expectations of a disorder-driven freezing of the otherwise dynamic moments in NaRuO<sub>2</sub>—an effect seen in a number of impurity-substituted spin liquid candidate materials [25, 39]. We note that this effect allows us to distinguish Fe incorporation into the lattice from trivial free Fe in the sample. While there may be a small fraction of Fe moments unincorporated, it is well below the background of the measurement. More extensive inclusions of Fe can be excluded via our diffraction measurements and the absence of detectable ferromagnetism at high temperature in isothermal magnetization measurements.

The susceptibility of NaRu<sub>1-x</sub>Fe<sub>x</sub>O<sub>2</sub> evolves in a manner suggestive of “swiss cheese” models proposed for impurity-substituted high-temperature superconducting cuprates [26, 40]. In cuprates, nonmagnetic Zn substitution into the copper oxide planes drives a local suppression of the superconducting ground state into patches of normal-state metals with a Zn-induced polarization of local Cu moments. In NaRuO<sub>2</sub>, the addition of magnetic Fe impurities into the Ru-plane seemingly locally suppresses the fluctuations of nearby Ru moments and polarizes them.

Monte Carlo simulations show that the susceptibil-

ity data are best fit with Ru moments polarized out to the next-nearest neighbors from the Fe-sites, leading to a relatively rapid polarization of all Ru moments by  $\approx 10\%$  site-substitution. This is consistent with the complete suppression of the  $\chi_0$  term in susceptibility at  $x = 0.1$ , and implies a connection between the enhanced  $\chi_0$  value of the parent NaRuO<sub>2</sub> compound and its bound/fluctuating Ru-moments. In parallel to the suppression of the  $\chi_0$  term, an enhanced, antiferromagnetic mean field  $\Theta_{CW}$  is resolved. This exchange field grows continuously in strength with added Fe content, consistent with a model of phase separation and percolating clusters of Fe-polarized Ru moments. Some caution should be given to the interpretation of the large  $\Theta_{CW}$  values obtained for larger  $x$  values. These values begin approaching the start of the temperature regime used to perform Curie-Weiss fits to the data, and, in the extreme  $x = 1$  NaFeO<sub>2</sub> limit, there is debate whether a Curie-Weiss model can be applied [28, 38]. An additional caveat is that our analysis is based on an assumed full polarization of each neighboring Ru moment, whereas our measurements cannot distinguish between this scenario and a partial polarization of a larger halo of Ru moments about each Fe site.

The Ru-induced moment in Fe-substituted NaRuO<sub>2</sub> invites comparison to the well-studied impurity effects in cuprates [41]. In the 2D copper oxide planes of cuprates, nonmagnetic substitution induces a local moment and the formation of a staggered polarization about the impurity site. A similar staggered polarization of some variety may form in NaRu<sub>1-x</sub>Fe<sub>x</sub>O<sub>2</sub> below its freezing temperature; however correlations above this temperature are not accessible with our current data. A notable difference between the ruthenate and cuprate cases is the nature of their parent Mott states, where within NaRuO<sub>2</sub>, a ferromagnetic ground state is predicted [18, 19]. This contrasts the antiferromagnetic Mott phase endemic to the cuprates and the nature of their impurity-induced spin correlations may differ. Another difference is the nature of the impurity dopants, where the magnetic impurity Fe differs from the nonmagnetic impurity-induced moments commonly studied in the cuprates. The apparent reduction of the local moment in magnetic impurity studies of the cuprates [42] versus the enhancement in NaRuO<sub>2</sub> likely arises from the differing local orbital physics of the  $e_g$  electrons in cuprates versus the  $t_{2g}$  orbital mixture in the ruthenate.

In summary, we have synthesized a series of magnetically doped NaFe<sub>x</sub>Ru<sub>1-x</sub>O<sub>2</sub> compounds. All compounds maintain the crystallographic structure of the parent compound, and an immediate spin freezing appears at the lowest level of Fe substitution attempted ( $x = 0.0125$ ). Susceptibility measurements identify a spin glass state that emerges with Fe-doping with a freezing temperature that conventionally increases with increased impurity content. A larger local moment is observed per Fe<sup>3+</sup> ion than that expected for  $S = 5/2$  impurities, and instead the local moment is best modeled via

Fe-impurities polarizing a radius of local  $J_{eff} = 1/2$  Ru-moments up to the next-nearest neighbor level. Our findings suggest a model of magnetic impurities locally suppressing the fluctuating or dimer-bound magnetic ground state of NaRuO<sub>2</sub>. Our data further support the hypothesis that the partial freezing observed in pristine NaRuO<sub>2</sub> arises from residual amounts of disorder in powders, likely in the form of Na substitutional disorder within the RuO<sub>2</sub> planes.

#### DATA AVAILABILITY

The raw supporting the findings of this study are openly available in Zenodo with

DOI:10.5281/zenodo.13750994.

#### V. ACKNOWLEDGMENTS

This work was supported by the US Department of Energy (DOE), Office of Basic Energy Sciences, Division of Materials Sciences and Engineering under Grant No. DE-SC0017752. The research made use of the shared facilities of the NSF Materials Research Science and Engineering Center at UC Santa Barbara (DMR- 1720256). The UC Santa Barbara MRSEC is a member of the Materials Research Facilities Network. ([www.mrfn.org](http://www.mrfn.org)). This work also used facilities supported via the UC Santa Barbara NSF Quantum Foundry funded via the Q-AMASE-i program under award DMR-1906325.

- 
- [1] D. I. Khomskii and T. Mizokawa, Orbitaly induced peierls state in spinels, *Phys. Rev. Lett.* **94**, 156402 (2005).
- [2] R. L. Dally, A. J. Heng, A. Keselman, M. M. Bordelon, M. B. Stone, L. Balents, and S. D. Wilson, Three-magnon bound state in the quasi-one-dimensional antiferromagnet  $\alpha$ -NaMnO<sub>2</sub>, *Physical Review Letters* **124**, 197203 (2020).
- [3] R. L. Dally, Y. Zhao, Z. Xu, R. Chisnell, J. W. Lynn, L. Balents, and S. D. Wilson, Amplitude mode in the planar triangular antiferromagnet Na<sub>0.9</sub>MnO<sub>2</sub>, *Nature communications* **9**, 2188 (2018).
- [4] C. Stock, L. C. Chapon, O. Adamopoulos, A. Lappas, M. Giot, J. W. Taylor, M. A. Green, C. M. Brown, and P. G. Radaelli, One-dimensional magnetic fluctuations in the spin-2 triangular lattice  $\alpha$ -NaMnO<sub>2</sub>, *Physical review letters* **103**, 077202 (2009).
- [5] T. M. McQueen, P. W. Stephens, Q. Huang, T. Klimczuk, F. Ronning, and R. J. Cava, Successive orbital ordering transitions in NaVO<sub>2</sub>, *Phys. Rev. Lett.* **101**, 166402 (2008).
- [6] J. A. Paddison, M. Daum, Z. Dun, G. Ehlers, Y. Liu, M. B. Stone, H. Zhou, and M. Mourigal, Continuous excitations of the triangular-lattice quantum spin liquid YbMgGaO<sub>2</sub>, *Nature Physics* **13**, 117 (2017).
- [7] Y. Shen, Y.-D. Li, H. Wo, Y. Li, S. Shen, B. Pan, Q. Wang, H. Walker, P. Steffens, M. Boehm, *et al.*, Evidence for a spinon fermi surface in a triangular-lattice quantum-spin-liquid candidate, *Nature* **540**, 559 (2016).
- [8] M. M. Bordelon, E. Kenney, C. Liu, T. Hogan, L. Posthuma, M. Kavand, Y. Lyu, M. Sherwin, N. P. Butch, C. Brown, *et al.*, Field-tunable quantum disordered ground state in the triangular-lattice antiferromagnet NaYbO<sub>2</sub>, *Nature Physics* **15**, 1058 (2019).
- [9] L. Ding, P. Manuel, S. Bachus, F. Grüßler, P. Gegenwart, J. Singleton, R. D. Johnson, H. C. Walker, D. T. Adroja, A. D. Hillier, *et al.*, Gapless spin-liquid state in the structurally disorder-free triangular antiferromagnet NaYbO<sub>2</sub>, *Physical Review B* **100**, 144432 (2019).
- [10] M. Baenitz, P. Schlender, J. Sichelschmidt, Y. Onykiienko, Z. Zangeneh, K. Ranjith, R. Sarkar, L. Hozoi, H. Walker, J.-C. Orain, *et al.*, NaYbS<sub>2</sub>: A planar spin-1 2 triangular-lattice magnet and putative spin liquid, *Physical Review B* **98**, 220409 (2018).
- [11] P.-L. Dai, G. Zhang, Y. Xie, C. Duan, Y. Gao, Z. Zhu, E. Feng, Z. Tao, C.-L. Huang, H. Cao, *et al.*, Spinon fermi surface spin liquid in a triangular lattice antiferromagnet NaYbSe<sub>2</sub>, *Physical Review X* **11**, 021044 (2021).
- [12] K. Ranjith, S. Luther, T. Reimann, B. Schmidt, P. Schlender, J. Sichelschmidt, H. Yasuoka, A. Strydom, Y. Skourski, J. Wosnitza, *et al.*, Anisotropic field-induced ordering in the triangular-lattice quantum spin liquid NaYbSe<sub>2</sub>, *Physical Review B* **100**, 224417 (2019).
- [13] B. R. Ortiz, M. M. Bordelon, P. Bhattacharyya, G. Pokharel, P. M. Sarte, L. Posthuma, T. Petersen, M. S. Eldeeb, G. E. Granroth, C. R. Dela Cruz, *et al.*, Electronic and structural properties of RbCeX<sub>2</sub> (X<sub>2</sub>: O<sub>2</sub>, S<sub>2</sub>, SeS, Se<sub>2</sub>, TeSe, Te<sub>2</sub>), *Physical Review Materials* **6**, 084402 (2022).
- [14] Z. Zhang, X. Ma, J. Li, G. Wang, D. Adroja, T. Perring, W. Liu, F. Jin, J. Ji, Y. Wang, *et al.*, Crystalline electric field excitations in the quantum spin liquid candidate NaYbSe<sub>2</sub>, *Physical Review B* **103**, 035144 (2021).
- [15] M. M. Bordelon, C. Liu, L. Posthuma, P. Sarte, N. Butch, D. M. Pajerowski, A. Banerjee, L. Balents, and S. D. Wilson, Spin excitations in the frustrated triangular lattice antiferromagnet NaYbO<sub>2</sub>, *Physical Review B* **101**, 224427 (2020).
- [16] G. Bastien, B. Rubrecht, E. Häußler, P. Schlender, Z. Zangeneh, S. Avdoshenko, R. Sarkar, A. Alfonsov, S. Luther, Y. A. Onykiienko, *et al.*, Long-range magnetic order in the triangular lattice antiferromagnet KCeS<sub>2</sub>, *SciPost Physics* **9**, 041 (2020).
- [17] B. R. Ortiz, P. M. Sarte, A. H. Avidor, A. Hay, E. Kenney, A. I. Kolesnikov, D. M. Pajerowski, A. A. Aczel, K. M. Taddei, C. M. Brown, C. Wang, M. J. Graf, R. Seshadri, L. Balents, and S. D. Wilson, Quantum disordered ground state in the triangular-lattice magnet NaRuO<sub>2</sub>, *Nature Physics* **19**, 943 (2023).
- [18] A. Razpopov, D. A. Kaib, S. Backes, L. Balents, S. D. Wilson, F. Ferrari, K. Riedl, and R. Valentí, A j<sub>1/2</sub> kitaev material on the triangular lattice: the case of NaRuO<sub>2</sub>, *npj Quantum Materials* **8**, 36 (2023).

- [19] P. Bhattacharyya, N. A. Bogdanov, S. Nishimoto, S. D. Wilson, and L. Hozoi, NaRuO<sub>2</sub>: Kitaev-heisenberg exchange in triangular-lattice setting, *npj Quantum Materials* **8**, 52 (2023).
- [20] S. Trebst and C. Hickey, Kitaev materials, *Physics Reports* **950**, 1 (2022).
- [21] R. V. Mishmash, J. R. Garrison, S. Bieri, and C. Xu, Theory of a competitive spin liquid state for weak mott insulators on the triangular lattice, *Phys. Rev. Lett.* **111**, 157203 (2013).
- [22] T. Grover, N. Trivedi, T. Senthil, and P. A. Lee, Weak mott insulators on the triangular lattice: Possibility of a gapless nematic quantum spin liquid, *Phys. Rev. B* **81**, 245121 (2010).
- [23] O. I. Motrunich, Variational study of triangular lattice spin-1/2 model with ring exchanges and spin liquid state in  $\kappa$ -ET<sub>2</sub> Cu<sub>2</sub> CN<sub>3</sub>, *Physical Review B—Condensed Matter and Materials Physics* **72**, 045105 (2005).
- [24] Y. Li, R. Seshadri, S. D. Wilson, A. K. Cheetham, and R. Valenti, Origins of temperature-dependent magnetism in open-shell 4d and 5d halide perovskites, arXiv preprint arXiv:2402.14064 (2024).
- [25] B. R. Ortiz, P. M. Sarte, A. H. Avidor, and S. D. Wilson, Defect control in the heisenberg-kitaev candidate material NaRuO<sub>2</sub>, *Physical Review Materials* **6**, 104413 (2022).
- [26] B. Nachumi, A. Keren, K. Kojima, M. Larkin, G. Luke, J. Merrin, O. Tchernyshöf, Y. Uemura, N. Ichikawa, M. Goto, *et al.*, Muon spin relaxation studies of Zn-substitution effects in high- T<sub>c</sub> cuprate superconductors, *Physical review letters* **77**, 5421 (1996).
- [27] See Supplementary Material at [URL].
- [28] T. McQueen, Q. Huang, J. W. Lynn, R. F. Berger, T. Klimczuk, B. G. Ueland, P. Schiffer, and R. J. Cava, Magnetic structure and properties of the  $s = 5/2$  triangular antiferromagnet  $\alpha$ -NaFeO<sub>2</sub>, *Phys. Rev. B* **76**, 024420 (2007).
- [29] T. Ichida, T. Shinjo, Y. Bando, and T. Takada, Magnetic properties of  $\alpha$ -NaFeO<sub>2</sub>, *Journal of the Physical Society of Japan* **29**, 795 (1970).
- [30] S. Shtrikman and E. Wohlfarth, The theory of the vogel-fulcher law of spin glasses, *Physics Letters A* **85**, 467 (1981).
- [31] A. Aharoni, The vogel-fulcher law of spin glasses, *Physics Letters A* **99**, 458 (1983).
- [32] V. K. Anand, D. T. Adroja, and A. D. Hillier, Ferromagnetic cluster spin-glass behavior in PrRhSn<sub>3</sub>, *Phys. Rev. B* **85**, 014418 (2012).
- [33] G. Benka, A. Bauer, P. Schmakat, S. Säubert, M. Seifert, P. Jorba, and C. Pfleiderer, Interplay of itinerant magnetism and spin-glass behavior in Fe<sub>x</sub>Cr<sub>1-x</sub>, *Phys. Rev. Mater.* **6**, 044407 (2022).
- [34] S. Chandra, H. Khurshid, W. Li, G. C. Hadjipanayis, M. H. Phan, and H. Srikanth, Spin dynamics and criteria for onset of exchange bias in superspin glass Fe /  $\gamma$ -Fe<sub>2</sub> O<sub>2</sub> core-shell nanoparticles, *Phys. Rev. B* **86**, 014426 (2012).
- [35] K. Vijayanandhini, C. Simon, V. Pralong, V. Caignaert, and B. Raveau, Spin glass to cluster glass transition in geometrically frustrated CaBaFe<sub>4-x</sub>Li<sub>x</sub>O<sub>7</sub> ferrimagnets, *Phys. Rev. B* **79**, 224407 (2009).
- [36] H. Khurshid, P. Lampen-Kelley, O. Iglesias, J. Alonso, M.-H. Phan, C.-J. Sun, M.-L. Saboungi, and H. Srikanth, Spin-glass-like freezing of inner and outer surface layers in hollow  $\gamma$ -Fe<sub>2</sub> O<sub>2</sub> nanoparticles, *Scientific Reports* **10.1038/srep15054**.
- [37] S. Mukherjee, A. Garg, and R. Gupta, Spin glass-like phase below 210K in magnetoelectric gallium ferrite, *Applied Physics Letters* **100**, 112904 (2012).
- [38] Z. Tomkowicz and B. van Laar, Magnetic properties and magnetic structure of  $\alpha$ -NaFeO<sub>2</sub>, *physica status solidi (a)* **23**, 683 (1974).
- [39] J. Guo, X. Zhao, S. Ohira-Kawamura, L. Ling, J. Wang, L. He, K. Nakajima, B. Li, and Z. Zhang, Magnetic-field and composition tuned antiferromagnetic instability in the quantum spin-liquid candidate NaYbO<sub>2</sub>, *Phys. Rev. Mater.* **4**, 064410 (2020).
- [40] S. Wakimoto, R. Birgeneau, A. Kagedan, H. Kim, I. Swainson, K. Yamada, and H. Zhang, Magnetic properties of the overdoped superconductor La<sub>2-x</sub>Sr<sub>x</sub>CuO<sub>4</sub> with and without zn impurities, *Physical Review B—Condensed Matter and Materials Physics* **72**, 064521 (2005).
- [41] H. Alloul, J. Bobroff, M. Gabay, and P. J. Hirschfeld, Defects in correlated metals and superconductors, *Rev. Mod. Phys.* **81**, 45 (2009).
- [42] P. Mendels, J. Bobroff, G. Collin, H. Alloul, M. Gabay, J. F. Marucco, N. Blanchard, and B. Grenier, Normal-state magnetic properties of ni and zn substituted in yba2cu3o6 + x: Hole-doping dependence, *Europhysics Letters* **46**, 678 (1999).